Numerical studies of bubble necking in viscous liquids

Shaoping Quan and Jinsong Hua*
Institute of High Performance Computing, 1 Science Park Road, #01-01 The Capricorn, Singapore Science Park II, Singapore 117528
(Received 26 December 2007; published 6 June 2008)

The pinch-off of a gas bubble from a tiny nozzle immersed vertically in another quiescent viscous fluid due to buoyancy is numerically investigated. The dynamics of bubble growth and pinch-off are described by the full Navier-Stokes equations for both gas and liquid phases. The equations are solved with a finite-volume method based on the SIMPLE scheme, coupled with a front tracking method to locate the interface between the two phases. The effects of liquid viscosity, surface tension, and gas density on the bubble pinch-off dynamics, which are always coupled in experiments, are investigated separately through simulations. The numerical results are compared with experimental observations on the bubble pinch-off for validation purposes. The simulation results show that the radius of the necking region decreases in a power law mode with time as $r \sim \tau^{\alpha}$, where τ is the time to pinch-off and the exponent α varies in the range 0.5–1.0 depending strongly upon the liquid properties such as viscosity and surface tension. In addition, the surface tension can significantly affect the bubble pinch-off exponent α when the surface tension coefficient is smaller than 0.030 N/m with a Bond number higher than 0.72. It is also found that both higher viscosity of the liquid phase and higher surface tension may result in a delayed pinch-off process and a larger bubble. The effect of gas phase density on the pinch-off is also investigated. As reported in the literature, the gas density variation has minimal effect on the necking process because the density ratio of the gas phase to the liquid phase is small.

DOI: 10.1103/PhysRevE.77.066303 PACS number(s): 47.55.df, 47.11.−j, 47.61.Jd, 47.10.ad

I. INTRODUCTION

Bubbles and drops exist widely in nature, our daily life, and industrial processes. Knowledge of the bubble and drop generation mechanism is one of the key essentials for understanding complex and important flow phenomena. Bubbles or drops are usually created through the pinch-off of the interface between two immiscible fluids. It has been a subject receiving considerable research interest for decades. For example, the breakup of a dense drop immersed in a background fluid of small or negligible viscosity (or density) has been extensively studied. Eggers [1] presented a comprehensive review of drop breakup. Investigations [2–4] showed that the power law of the filament necking radius and the geometric shape of the filament are universal.

However, the recent experimental work by Doshi *et al.* [5] on the pinch-off of a drop with low viscosity inside a much more viscous fluid revealed that the universality, which had been proven valid in the pinch-off process of a viscous liquid drop in a less viscous or inviscid background fluid, breaks down in their configuration. This indicates that the dynamics of gas bubble pinch-off in a viscous liquid is different from that of liquid drop dripping in gas. The bubble pinch-off in a viscous liquid is receiving more and more research interest. Keim *et al.* [6] studied the behavior of an air bubble detaching from an underwater nozzle using a high-speed video camera. Their observations showed that, for air bubble breakup in water, a small asymmetry in the initial condition is preserved throughout the whole breakup process because the surface tension is not the driving factor for the breakup, so the universality is lost. Burton *et al.* [7] reported experimental studies on the pinch-off of gas bubbles in viscous liquids with a wide range of viscosity, using a video of 100 000 frames per second (fps). Three regimes of gas bubble pinch-off behavior were found depending upon the background liquid viscosity: (1) the radius (r) of the neck region decreases linearly with the time to pinch-off ($\tau = t_p - t$, where t denotes time, and t_p stands for the time at pinch-off) for a bubble in a high-viscosity fluid, $r \sim \tau$; (2) for a bubble in a low-viscosity fluid, the radius of the pinch neck decreases as $r \sim \tau^{1/2}$; and (3) for a bubble immersed in an intermediate-viscosity fluid, a long and thin thread is discovered. Extensive experimental studies by Thoroddsen *et al.* [8] investigated the dynamics and the shape of the neck region while an air bubble pinches off slowly in various glycerin-water mixtures driven by buoyancy using an ultrahigh-speed video with up to one million fps. The effects of liquid viscosity on the pinch-off speed and neck shape are characterized. For gas bubble pinch-off in water, the radius of the neck decreases with a power law behavior $r \sim \tau^{\alpha}$ with an exponent in the range of $\alpha = 0.57 \pm 0.03$, which is slightly larger than one-half predicted by Rayleigh-Plesset theory [7]. The pinch-off speed starts to slow down at a viscosity of about ten times that of water. A further increment of liquid viscosity also leads to a change in the power law. The power law exponent (α) increases and approaches 1.0 for viscosity higher than 70 cP. Thoroddsen *et al.* also found that the variation of gas density has a minimal effect on the bubble pinch-off. In general, the experimental results [7,8] about the effects of liquid viscosity on gas bubble pinch-off in viscous liquids agree well. The evolution of the bubble profile is not well understood so far since the pinching-off mechanism is governed by the balancing of the gravitational force, viscous stress, surface tension, flow inertia, and hydrostatic pressure [5]. Due to the difficulty of isolating the effects of surface tension in experiments, there are very limited reports of experimental studies on the effects of surface tension on bubble

*Author to whom correspondence should be addressed. FAX: 65-67780522. huajs@ihpc.a-star.edu.sg

pinch-off behavior despite its important role. In addition, a careful study of the previous works as shown in Fig. 5 of Burton *et al.* [7] and Fig. 5 of Chen *et al.* [3] shows that there is a significant transition of the power law exponent when the neck radius is about 100–150 μm during the pinch-off process of a bubble or droplet. Chen *et al.* [3] explained this change as due to a transition from potential to inertial viscous flow. However, a better understanding about the transition of the power law exponent around the neck radius of 150 μm with bubble pinch-off in an intermediate-viscous liquid has not been established so far; here the assumptions for both potential flow and Stokes flow may become invalid.

Early work by Longuet-Higgins *et al.* [9] studied the bubble growth and detachment from an underwater nozzle analytically based upon the balance of pressure and capillary force in the limit of very low gas flow rate (quasistatic limit). Oguz and Prosperetti [10] presented a numerical modeling approach, a boundary integral potential calculation, to analyze bubble growth and departure from a submerged needle under different gas flow rates. Although they neglected viscous effects, the simulation showed remarkable agreement with the earlier experiment reported in [9]. Wong *et al.* [11] and Sierou and Lister [12] also used a boundary integral method to study the viscous capillary pinch-off and its self-similarity. Using a slender-body theory, Eggers *et al.* [13] theoretically investigated the collapse of an axisymmetric bubble inside a fluid with low viscosity, and proposed a correction of the power law exponent, i.e., $\alpha=1/2+1/(4\sqrt{-\ln\tau})$. Axisymmetric bubble pinch-off at high Reynolds numbers was also studied by Gordillo and co-workers [14,15], and they found that the bubble pinching neck radius r varies with τ as $\tau\sim r^2\sqrt{-\ln r^2}$. Bergmann *et al.* [16] investigated the breakup of a giant bubble and they found that the collapse is not self-similar in a strict sense for a finite Froude number. They also proposed that the radius evolution of the neck region is only a function of the Froude number. A bubble or drop in a straining flow at high Reynolds numbers was studied by Rodriguez-Rodriguez *et al.* [17] with the assumption of axisymmetric and irrotational flow. They found that a bubble breaks only if the inertia of the continuous flow is sufficiently large to overcome the surface tension, and the breakup time depends only on the Weber number. Hence, the above-mentioned complex bubble pinch-off behavior and dynamics actually result from the combined effects of viscous stress, capillary force, inertia, and pressure. Most of the previous numerical methods and analytical approaches are suitable for certain flow regimes that are dominated by one or two kinds of force. The majority of the previous work on bubble pinch-off in another more viscous fluid was experimental and analytical, and most of the numerical solutions were based on the inviscid assumption. With the rapid advance of numerical methods and affordable computing resources, the solution of the full Navier-Stokes equation for multiphase flows is becoming one of the promising alternative approaches to understanding the detail of the bubble pinch-off dynamics for wider flow regimes.

Suryo *et al.* [18] used a finite-element method to study the dynamics of an annular compound jet whose core is inviscid gas and whose shell is a liquid of finite viscosity. By solving the Navier-Stokes equation for the gas phase with the proper boundary condition on the interface, they showed that the pinch-off dynamics is linear, non-self-similar, and nonuniversal. Gerlach *et al.* [19] applied a combined volume-of-fluid and level-set method to simulate the process of bubble formation, detachment, and rise from a submerged orifice with a constant gas flow rate in an axisymmetric coordinate system. The influences of fluid properties (density, viscosity, surface tension) were examined individually.

In this paper, numerical simulations are applied to analyze the buoyancy-driven pinch-off of a gas bubble from a tiny nozzle immersed in another quiescent viscous fluid. The two-dimensional axisymmetric Navier-Stokes equations for both gas and liquid phases are solved by a finite-volume scheme, and the bubble shape is captured with an improved front tracking method [20,21]. The temporal variations of bubble shape during bubble growth and pinch-off predicted by simulations are compared with experimental observations in both time and spatial domains. Special attention is focused on the accuracy of numerical predictions on the bubble necking and pinch-off, and good agreement is achieved over a large range of experimental conditions with different liquid viscosities. The effect of the density ratio, viscosity ratio, and surface tension on the dynamics of two-phase flows, such as the bubble rising and droplet dynamics, is an interesting subject for researchers in the field [22–24]. In this paper, by varying only one of the fluid properties such as liquid viscosity, the surface tension coefficient, and bubble density in each simulation, the effects of these three factors on the bubble breakup dynamics are investigated separately, which is a challenge in experiments but important in understanding the physics. It is found that both viscosity and surface tension play significant roles in the bubble breakup, while the effect of bubble density is minimal. Higher surface tension or viscosity tends to slow down the pinch-off process and to create larger bubbles.

II. NUMERICAL METHOD AND PROBLEM FORMULATION

The physical problem of a bubble pinch-off from a capillary nozzle submerged in a viscous liquid due to buoyancy is sketched in Fig. 1. In the present study, the capillary nozzle has a radius of $r_o=1.35\times10^{-3}$ m. The simulation domain indicated as the gray zone in Fig. 1 has a radius of $3r_o$ and a height of $12r_o$. The densities of the bubble phase and the outer liquid are ρ_g and ρ_l, respectively, and the viscosities of the two phases are μ_g and μ_l, respectively. The density ratio is defined as $\eta=\rho_g/\rho_l$, and the viscosity ratio as $\lambda=\mu_g/\mu_l$. The bubble top rising distance x is also illustrated in Fig. 1 as the length from the top tip of the bubble to the nozzle exit, and r represents the neck radius. The two fluids are assumed to be immiscible and incompressible, and the problem is assumed to be axisymmetric as the bubble grows at a very slow rate, about 10 s for release of one bubble. The initial flow fields for both liquid and gas phases are assumed to be stationary. The initial position of the gas-liquid interface is assumed flat at the capillary nozzle outlet. A no-slip boundary condition is applied to the outer walls. As the problem is buoyancy driven, the flow rate through the nozzle is kept low

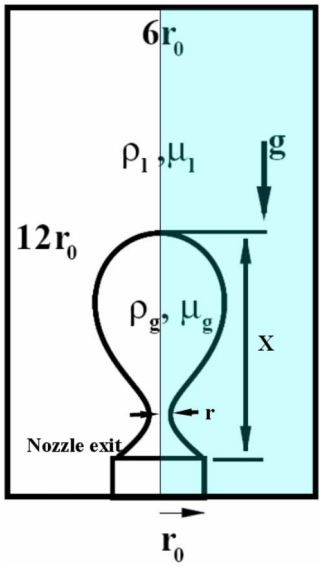

FIG. 1. (Color online) Schematic diagram of a bubble pinch-off from a capillary tube ($r_o = 1.35 \times 10^{-3}$ m) submerged in a viscous liquid due to buoyancy. Here, r represents the bubble neck radius. The bubble top rising distance (x) is shown as the length from the bubble top tip to the nozzle exit.

to minimize any inertial effect. The governing equations for the fluid flow system are

$$\nabla \cdot \mathbf{u} = 0, \tag{1}$$

$$\frac{\partial(\rho \mathbf{u})}{\partial t} + \nabla \cdot \rho \mathbf{u}\mathbf{u} = -\nabla p + \nabla \cdot [\mu(\nabla \mathbf{u} + \nabla \mathbf{u}^T)] + \int \sigma \kappa_f \mathbf{n}_f \delta(\mathbf{x} - \mathbf{x}_f) ds_f + (\rho - \rho_l)\mathbf{g}, \tag{2}$$

where $\mathbf{u}$ is the fluid velocity, p denotes pressure, ρ stands for the density and μ for the viscosity of the medium, $\mathbf{g}$ is the gravitational acceleration, s_f denotes the arc length measured on the interface, κ_f stands for the curvature of the interface, σ is the surface tension coefficient and is assumed to be a constant to avoid Marangoni effects, $\mathbf{n}$ stands for the unit normal vector on the interface, $\mathbf{x}$ is the position vector on the interface, and $\delta(\mathbf{x}-\mathbf{x}_f)$ stands for the delta function that is nonzero only when $\mathbf{x}=\mathbf{x}_f$.

We nondimensionalize the equations by introducing dimensionless characteristic variables as follows:

$$\mathbf{x}^* = \frac{\mathbf{x}}{r_o}, \quad \mathbf{u}^* = \frac{\mathbf{u}}{\sqrt{g r_o}}, \quad t^* = \sqrt{\frac{g}{r_o}} t, \quad \rho^* = \frac{\rho}{\rho_l},$$

$$p^* = \frac{p}{\rho_l g r_o}, \quad \mu^* = \frac{\mu}{\mu_l}, \quad \kappa^* = r_o \kappa, \quad \mathbf{g}^* = \frac{\mathbf{g}}{g},$$

where r_o is the radius of the capillary nozzle and $g = \|\mathbf{g}\|$. Thus we may reformulate the Navier-Stokes equations as

$$\nabla \cdot \mathbf{u}^* = 0, \tag{3}$$

$$\frac{\partial(\rho^* \mathbf{u}^*)}{\partial t^*} + \nabla \cdot \rho^* \mathbf{u}^* \mathbf{u}^* = -\nabla p^* + \frac{1}{\mathrm{Ar}} \nabla \cdot [\mu^*(\nabla \mathbf{u}^* + \nabla^{\mathrm{T}} \mathbf{u}^*)] + \frac{1}{\mathrm{Bo}} \int_\Gamma \kappa_f^* \mathbf{n}_f \delta(\mathbf{x}^* - \mathbf{x}_f^*) ds_f + (\rho^* - 1)\mathbf{g}^*. \tag{4}$$

The Archimedes number (Ar) and Bond number (Bo) used here are thus defined as

$$\mathrm{Ar} = \frac{\rho_l g^{1/2} r_o^{3/2}}{\mu_l} \quad \text{and} \quad \mathrm{Bo} = \frac{\rho_l g r_o^2}{\sigma}.$$

Hence, the problem of bubble pinch-off can be specified by four nondimensional numbers such as the density ratio ($\eta = \rho_g / \rho_l$), viscosity ratio ($\lambda = \mu_g / \mu_l$), Archimedes number, and Bond number. The Archimedes number denotes the importance of the buoyancy force over viscous force, and the Bond number represents the relative importance of the buoyancy and surface tension forces.

The numerical method solves one set of Navier-Stokes equations (3) and (4) by treating the two phases as one fluid with variable material properties. Here, only a brief review of the method is given, and the details of the method are described in [21]. The fluid properties are set and smoothed according to the position of the interface. Surface tension is computed on the front and then distributed to the fixed grid using the Dirac δ function [25,26]. The unsteady Navier-Stokes equations are solved by a finite-volume method using an improved SIMPLE scheme [27]. By applying this semi-implicit scheme, the numerical method is more robust for solving two-phase flow problems with large density and viscosity differences. The interface is advected using the velocity interpolated from the neighboring flow field. The front mesh size is adapted through coarsening and refining to deal with the bubble front deformation. The numerical method was tested and validated by a number of rising bubble cases [21].

In the current study, a uniform Cartesian mesh grid of 360×90 has been used to discretize the simulation domain for the axisymmetric model as shown in Fig. 1. The radius of the nozzle outlet is resolved with 30 grid points. In addition, a constant, nondimensionalized time step (Δt^*) around 0.01 is used in the simulation. Each simulation takes about 11 000 time steps to predict the overall bubble growth from the initial gas injection to final bubble pinch-off, while the pinch-off process from necking to breakup normally takes about 100–300 time steps. The simulation is performed on a SGI Altix 3700 computer using one processor. The simulation time for one case normally takes about 20–30 CPU hours.

III. RESULTS AND DISCUSSION

In this section, the numerical method is first validated against the experimental results of Thoroddsen *et al.* [8] for the simulation of bubble pinch-off. Then, by varying only one property of the fluids a time, we investigate the effects of the bulk fluid viscosity, the surface tension, and the bubble phase density on the bubble pinch-off dynamics.

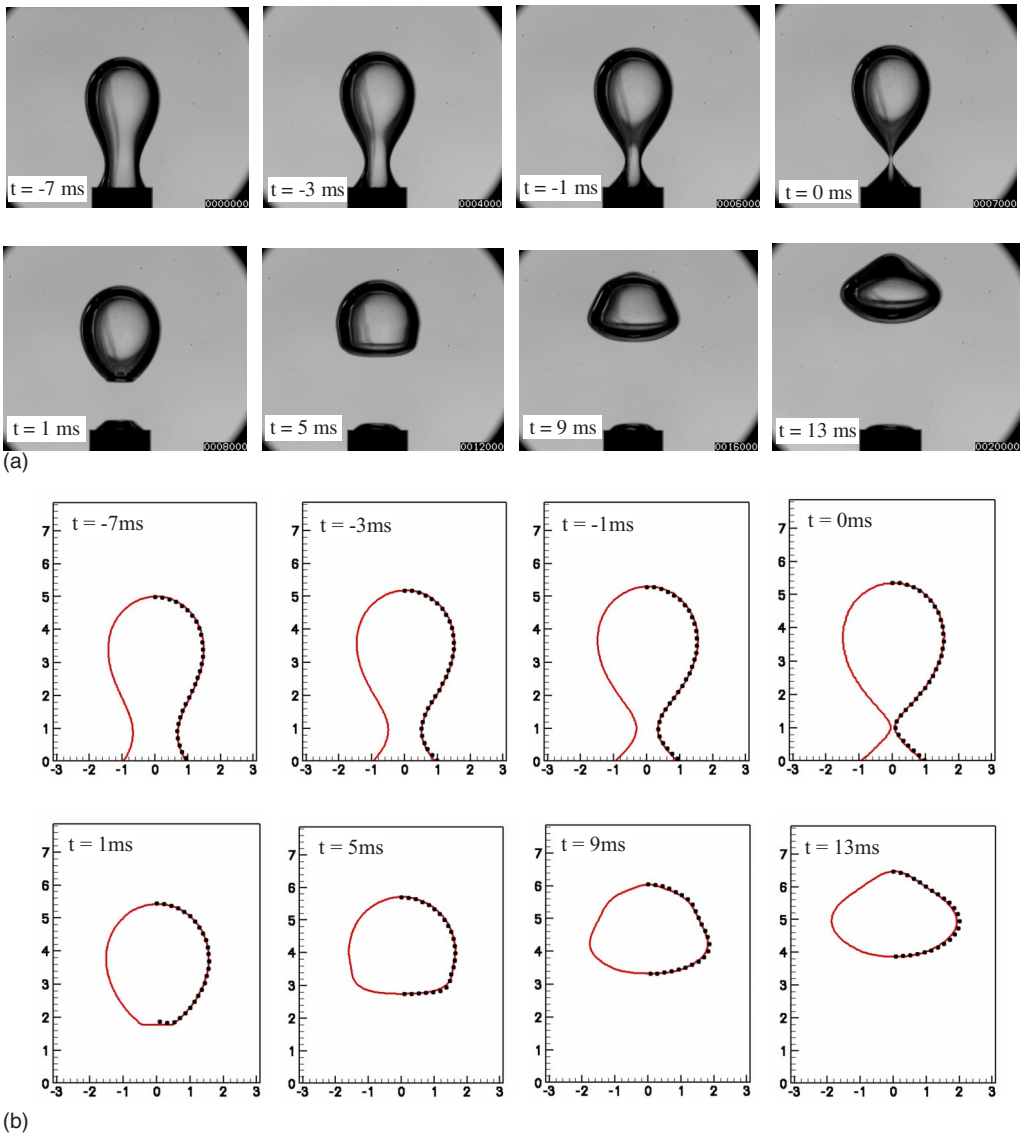

FIG. 2. (Color online) (a) Snapshots of the experimentally observed air bubble pinch-off process in water; (b) comparison of the bubble shapes predicted by simulation (dotted line) and observed in experiments (solid line). Both experiment and simulation were performed under the conditions $r_o=1.35\times10^{-3}$ m, $\rho_g=1.005$ kg/m^3, $\rho_l=1.0\times10^3$ kg/m^3, $\mu_g=0.0142$ cP, $\mu_l=1.48$ cP, $\sigma=6.5\times10^{-2}$ N/m, and $g=9.8$ m/s^2.

A. Validation of numerical method

Experimental observations of an air bubble released from a nozzle submerged in water were reported in the early experimental work of Longuet-Higgins *et al.* [9]. The later numerical study by Oguz and Prosperetti [10] predicted the bubble growth and pinch-off dynamics by means of a boundary-integral potential flow calculation, neglecting the viscous effects and assuming the flow to be irrotational. In this paper, we predict the bubble pinch-off by solving the full Navier-Stokes equations for both the bubble and the liquid phases. Figure 2(a) shows the experimentally observed air bubble pinch-off process in water by Thoroddsen *et al.* [8]. The bubble shape variation during the pinch-off process predicted by the current simulation is shown in Fig. 2(b), with a direct comparison with the experiments. The simulation and experiment were performed under the same condition: $r_o=1.35\times10^{-3}$ mm, $\rho_g=1.005$ kg/m^3, $\rho_l=1.0\times10^3$ kg/m^3, $\mu_g=0.0142$ cP and $\mu_l=1.48$ cP, $\sigma=6.5\times10^{-2}$ N/m, and $g=9.8$ m/s^2. It can be concluded from Fig. 2(b) that the agreement between the numerical predictions and experimental observations is quite good in both spatial and time domains.

In order to test the accuracy and robustness of the numerical method, numerical predictions of bubble pinch-off were validated against the experiments over a range of liquid viscosities, rather than just one specific condition. A number of simulations have been conducted in this study according to the exact experimental conditions as reported by Thoroddsen *et al.* [8] to investigate the effects of liquid viscosity on bubble pinch-off behavior. In fact, in their series of experiments, not only was the liquid viscosity changed, but also the other liquid properties, e.g., the liquid density and the surface tension coefficient may vary slightly with the concentration

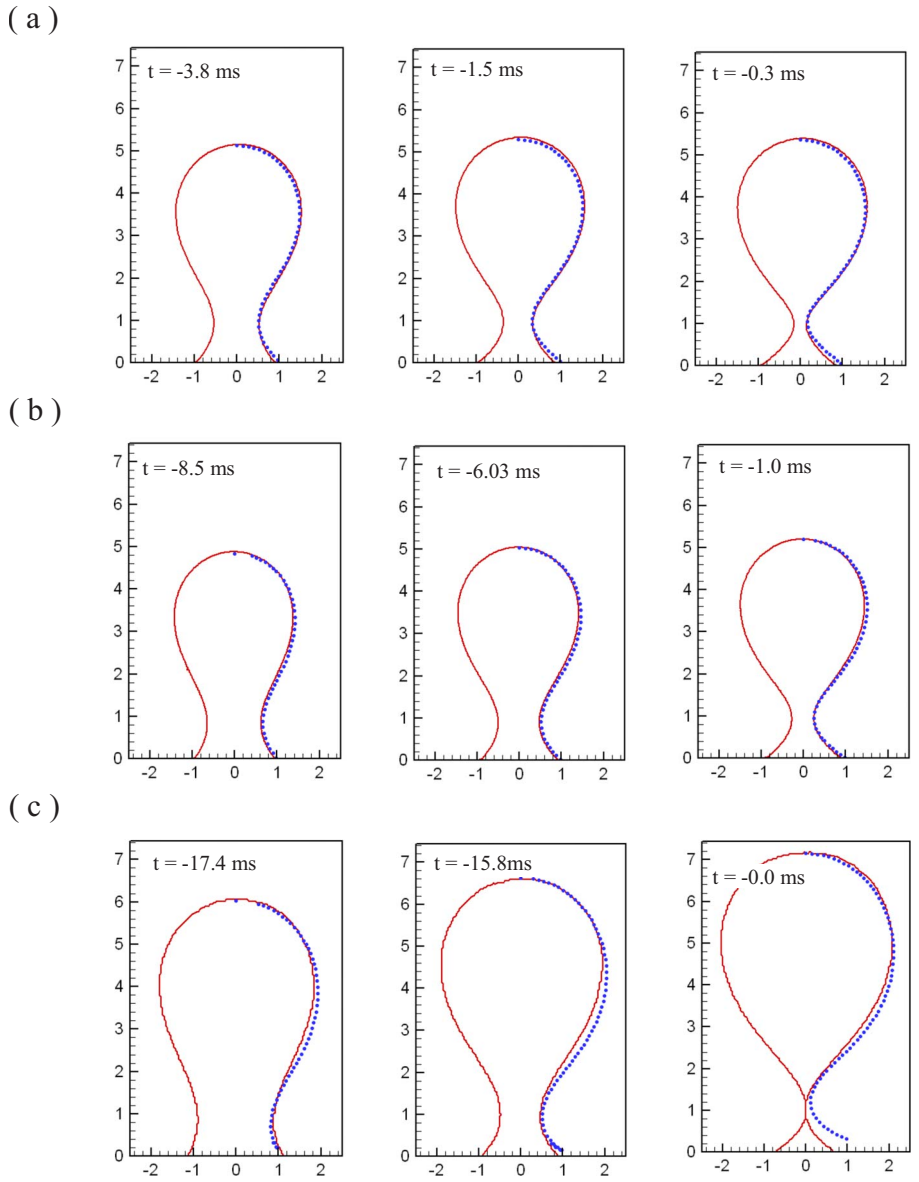

FIG. 3. (Color online) Comparison of the temporal variations of bubble shapes before bubble pinch-off predicted by simulations (dotted line) and observed in experiments (solid line) under the conditions of different glycerin-water compositions, (a) 75% glycerin and 25% water (μ_l=26 cP); (b) 84% glycerin and 16% water (μ_l=68 cP); and (c) 99% glycerin and 1% water (μ_l=3400 cP).

of the water-glycerin mixtures and the environmental temperature. Figure 3 shows a comparison of the variation of bubble shapes before pinch-off predicted by simulations (dotted line) and observed in experiments (solid line) under conditions of different mixture compositions: Fig. 3(a), 75% glycerin and 25% water (μ_l=26 cP); Fig. 3(b), 84% glycerin and 16% water (μ_l=68 cP); and Fig. 3(c), 99% glycerin and 1% water (μ_l=3400 cP). It can be seen from Fig. 3 that our simulated bubble shapes agree well with the experimental observations within a large range of fluid viscosity. This comparison further validates the accuracy of our numerical method. And this numerical method is further applied to investigate the effects of the viscosity, the surface tension coefficient, and the gas density on the bubble pinch-off dynamics.

In addition, a detailed comparison of the necking history of the neck radius during pinch-off between the experimental results and the numerical simulations is shown in Fig. 4, with an inset showing a zoomed-in view for the period when the pinch-off process occurs during $0 \leq \tau \leq 4000$ μs. The parameters for this case are $\sigma = 6.5 \times 10^{-2}$ N/m, $\rho_l = 1200$ kg/m^3, $\rho_g = 1.0$ kg/m^3, $\mu_g = 0.01$ cP, and $\mu_l = 68$ cP. In experiments, the bubble pinch-off process was recorded twice using different video capturing speeds, 2000 fps for the overall process and 100 000 fps for the detailed process at the pinch-off point. As shown in Fig. 4, the agreement for neck radius greater than 110 μm is excellent, which further validates the good accuracy of our numerical method. It should be noted that, due to the current numerical technology and the limited available computational resources, it is a challenge to continue the simulation when the neck radius is smaller than 110 μm (8% of the nozzle radius). With the current numerical method, in order to accurately capture the physics at the pinch-off region for a radius smaller than 110 μm, a very fine mesh is needed. In order to capture the bubble growth behavior, a large computational domain is necessary. In addition, the actual pinch-off process happens within a shorter time compared to the bubble growth, so that the time step should be small enough to resolve the physics. Thus, the computational time will be significantly increased

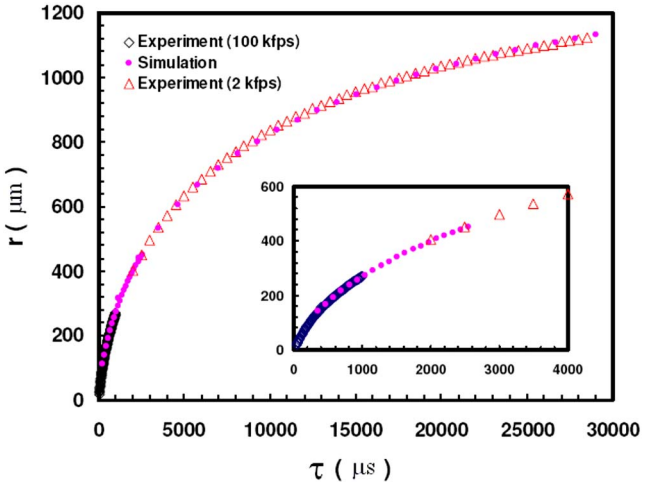

FIG. 4. (Color online) Detailed comparison of the necking radius between the experiments and the numerical simulation. Ar =2.7, Bo=0.36, ρ_l=1200 kg/m^3, ρ_g=1.0 kg/m^3, μ_g=0.01 cP, and μ_l=68 cP.

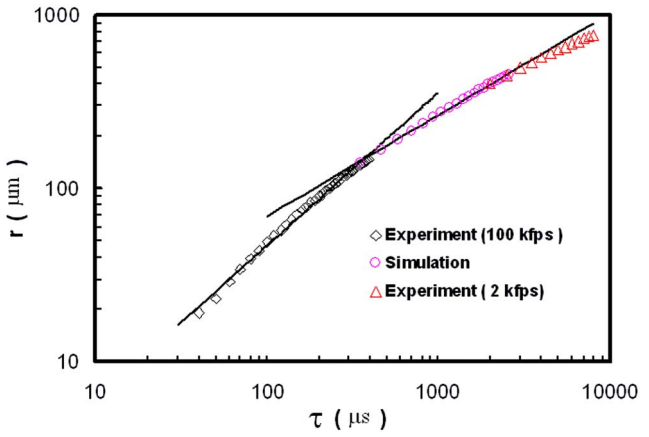

FIG. 5. (Color online) Power law curving fitting for experimental results and the numerical simulations. It shows $r \sim t^{0.88}$ when $r<110$ μm, and $r \sim t^{0.58}$ when $110<r<500$ μm. Ar=2.7, Bo=0.36, ρ_l=1200 kg/m^3, ρ_g=1.0 kg/m^3, μ_g=0.01 cP, and μ_l=68 cP.

by solving the full Navier-Stokes equations in a domain 16 mm in length and 8 mm in width with higher resolution in both time and space. An adaptive mesh method and parallel computing could be used to address this challenge; this is our ongoing research project, and we will address this in future work. Figure 5 shows the power law curve fittings for the experimental results (using 100 000 fps) with a neck radius less than 148 μm, and for both the numerical simulations and experimental results (using 2000 fps) with a neck radius greater than 110 μm, respectively. The two fitted curves have different slopes, and the slope for the numerical simulation ($110<r<500$ μm) is smaller than the experimental one ($r<148$ μm). The slope is 0.88 for the experimental results obtained at the video capturing speed of 100 000 fps, and 0.58 for the numerical predictions. A comparison with the previous work of Burton *et al.* [7] and Chen *et al.* [3] shows that a similar transition of the power law fitting exponent is also found in their pinch-off studies of bubble and droplet. As mentioned previously, due to the limitation of the current available numerical technique and the limited computational resources, all the power law fittings obtained from the simulation results discussed hereafter are performed for the neck radius varying in the range of $110<r<500$ μm during bubble pinch-off.

B. Viscosity effects

As we are interested in a low-viscosity bubble pinching off inside a more viscous fluid (e.g., an air bubble in water), the viscosity of the liquid phase will affect the bubble pinch-off dynamics to some extent. Burton *et al.* [7] studied the viscosity effect on the bubble breakup using different fluids. They found that the bulk fluid viscosity affects the breakup process and results in three different regimes. However, the surface tension coefficient varies within a factor of 2 of the surface tension of water in their experiments. By changing the concentration of the water-glycerin mixture, Thoroddsen *et al.* [8] investigated the liquid viscosity effect on the bubble breakup dynamics. However, the Bond number is not a constant in their experiments due to the fact that the density and surface tension coefficient of the mixture may change with the glycerin and water concentrations in the mixture. In our numerical simulations, by varying the liquid phase viscosity but keeping other fluid properties constant, we can investigate the effect of viscosity alone on the bubble pinch-off dynamics.

Figure 6 shows the neck radius versus time before bubble pinch-off for a wide range of viscosities, i.e., μ_l=4.2, 6.8, 17, 68, 340, and 850 cP. The bubble phase viscosity is kept as a constant of 0.01 cP. The symbols stand for the numerical results shoown on a logarithmic scale, while the lines denote the fitted curves using a power law. In this study, the Bond number is fixed to be 0.36, and the density ratio is 8.3×10^{-4} for all the simulations. The corresponding viscosity ratios λ are 2.4×10^{-3}, 1.5×10^{-3}, 5.9×10^{-4}, 1.5×10^{-4}, 2.9×10^{-5}, and 1.2×10^{-5}, respectively. It can be seen from Fig. 6 that the radius of the neck region decreases with time as a power law, as the fitted lines are straight in the log-log plot. Figure 7 depicts the variation of exponent α versus the liquid phase viscosity. It is found that the exponent α varies with the fluid viscosity μ_l differently in three regimes. A small exponent ($\sim$0.55) is obtained for the low-viscosity case ($\mu_l<68$ cP), and a large exponent ($\sim$0.95) for high viscosity ($\mu_l>500$ cP). A transition of the exponent α from the small value to the large value is found in the viscosity range of $68<\mu_l<500$ cP. Overall, the results are in qualitative agreement with those reported in [7] and [8]. However, it should be noted that there are some differences in the power law exponents when the results obtained from the current simulation are compared with those from the experiments. According to Burton *et al.* [7], there is a sharp change of the exponent for the liquid viscosity in the range of 10–100 cP, while a smoother change is found by Thoroddsen *et al.* [8]. It can be seen from Fig. 7 that the significant change of the power law exponent occurs when $68<\mu_l<500$ cP, and the change is rather smooth. As stated in the previous section, this difference between the simulation prediction and

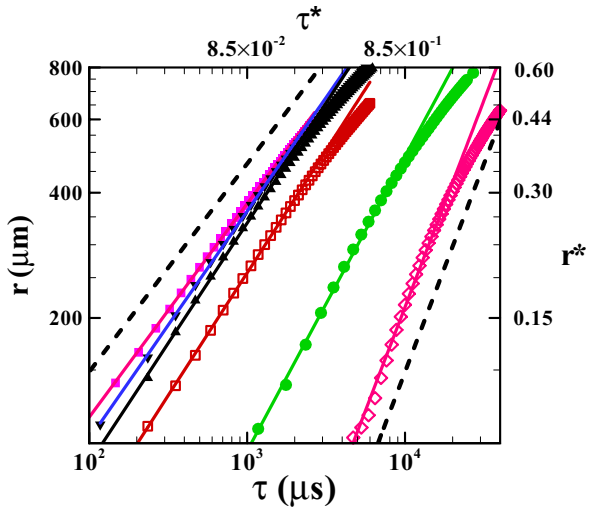

FIG. 6. (Color online) Effect of liquid viscosity on the bubble neck radius (r) shrinkage with time (t) during pinch-off. The nondimensional time (τ^*) and radius (r^*) are also shown. The liquid viscosity changes at μ_l=4.2 (■), 6.8 (▼), 17.0 (▲), 68.0 (□), 340.0 (●), and 850.0 cP (◇), and the slopes of the fitted lines are 0.51, 0.55, 0.58, 0.59, 0.71, and 0.95, respectively. The corresponding Archimedes numbers (Ar) are 44.3, 27.4, 11.0, 2.74, 0.5, and 0.2. The corresponding viscosity ratios are 2.4×10^{-3}, 1.5×10^{-3}, 5.9×10^{-4}, 1.5×10^{-4}, 2.9×10^{-5}, and 1.2×10^{-5}. The top and bottom dashed lines have slopes of 0.5 and 1.0, respectively. Other parameters are fixed as Bo=0.36, η=8.3×10^{-4}; ρ_l=1200 kg/m^3, ρ_g=1.0 kg/m^3, μ_g=0.01 cP, and r_o=1.35×10^{-3} m.

experimental observation reported in [7,8] is mainly due to the power law fitting for the numerical simulation results is done for the neck radius in the range of $110<r<500$ μm, while experimental results is obtained for the neck radius in the range of $r<148$ μm, as illustrated in Fig. 5.

When the surface tension coefficient is fixed in all the simulations, the other two major competing forces are buoyancy and viscous force. In order to evaluate the importance of the two forces, a modified Archimedes (Ar′) number is

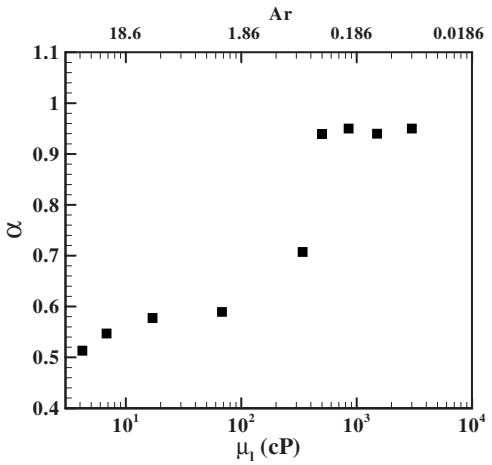

FIG. 7. Variation of power law exponent (α) versus the liquid viscosity μ_l and Ar. Other parameters are fixed as Bo=0.36, ρ_l=1200 kg/m^3, ρ_g=1.0 kg/m^3, μ_g=0.01 cP, and r_o=1.35×10^{-3} m.

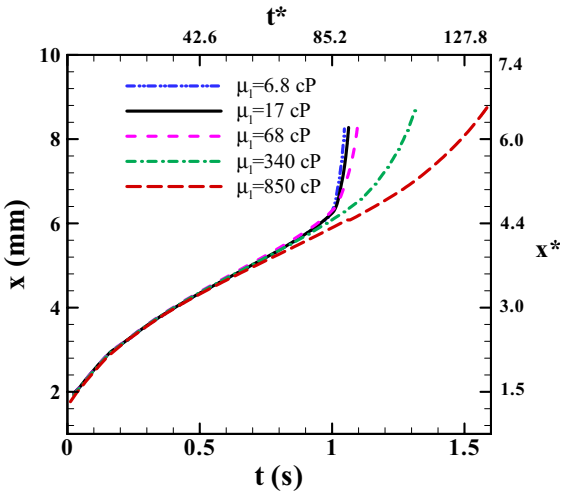

FIG. 8. (Color online) Effect of liquid viscosity on the bubble top rising distance with time during pinch-off. The nondimensional time (t^*) and top rising distance (x^*) are also shown. The viscosity ratios are 2.4×10^{-3}, 1.5×10^{-3}, 5.9×10^{-4}, 1.5×10^{-4}, 2.9×10^{-5}, and 1.2×10^{-5}. Other parameters are fixed as Bo=0.36, ρ_l=1200 kg/m^3, ρ_g=1.0 kg/m^3, μ_g=0.01 cP, and r_o=1.35×10^{-3} m.

introduced as $\mathrm{Ar}'=(\rho_l-\rho_g)g^{1/2}r_o^{3/2}/\mu_l$, which stands for the ratio between buoyancy force and viscous force. Since $\rho_l \gg \rho_g$, $\mathrm{Ar}'\approx A_r=\rho_l g^{1/2}r_o^{3/2}/\mu_l$. A similar definition of the Archimedes number is also adopted in the previous work of Bonometti and Magnaudet [28]. Figure 7, where Ar is plotted on the top x axis, also shows the variation of the exponent α versus Ar. It can be clearly seen from Fig. 7 that a great change in exponent occurs when $0.37<\mathrm{Ar}<2.7$, i.e., $O(1)$. This indicates that the liquid viscosity has significant effects on the bubble pinch-off process, and thus affects the power-law exponents (α) in a noticeable way. For large viscosity $\mu_l>500$ cP where $\mathrm{Ar}\ll O(1)$, the bubble neck shrinks linearly with the pinch-off time. While for the low liquid viscosity $\mu_l<68$ cP where $\mathrm{Ar}\gg O(1)$, the effect of viscosity force on the bubble pinch-off will become less significant since the power law exponent varies in a small range of 0.5–0.6 as shown in Fig. 7. The balance between the surface tension force and the buoyancy force will be the dominant factor in controlling the bubble pinch-off process.

Figure 8 shows the effect of viscosity on the bubble top rising distance (x) with time during pinch-off. For the low-viscosity cases, a transition point, where the slope of the curve changes rapidly, can be found in Fig. 8. Before this transition point, the bubble growth is dominated by the surface tension and buoyancy force. After the transition point, the bubble size is big enough, and it starts to neck and pinch off. As the bubble neck radius is reduced and the surface tension effect on the bubble top rising becomes minimal, the bubble top rises quickly as a result of the strong buoyancy force and the low viscous force. On the other hand, when the liquid viscosity is high, the bubble rises smoothly, and no sharp transition point is observed. This is due to the high liquid viscosity which retards the bubble pinch-off process significantly. A careful study of Fig. 8 shows that the viscosity has minimal effect on the bubble top rising distance at the

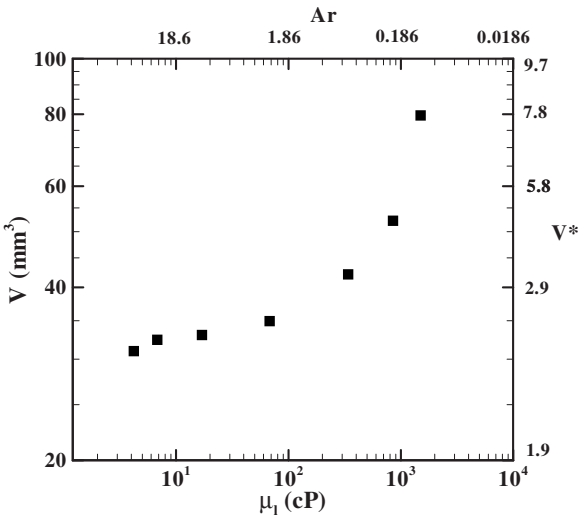

FIG. 9. Variation of bubble volume versus the liquid viscosity μ_l and Ar. The nondimensional volume (V^*) is also shown, and it is nondimensionalized by the volume of a sphere with the nozzle exit radius. Other parameters are fixed as Bo=0.36, ρ_l=1200 kg/m^3, ρ_g=1.0 kg/m^3, μ_g=0.01 cP, and $r_o=1.35\times10^{-3}$ m.

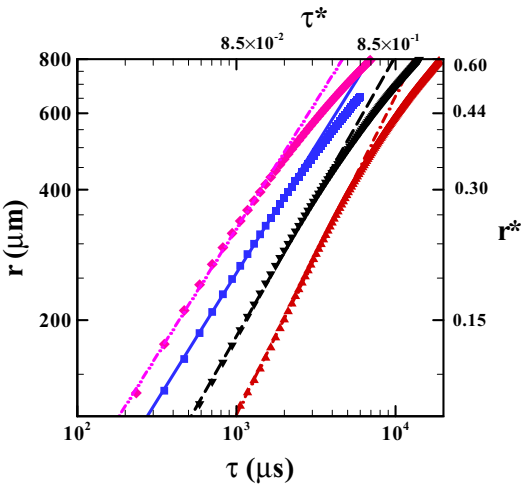

FIG. 10. (Color online) The effect of surface tension coefficient on the bubble neck shrinkage with time during bubble pinch-off. The nondimensional time (τ^*) and radius (r^*) are also shown. The surface tension coefficient varies at σ=120 (♦), 60 (■), 30 (▼), 15 (▲) mN/m, and the corresponding Bond numbers are 0.18, 0.36, 0.71, and 1.43, respectively. The slopes for the four fitted lines are 0.58, 0.59, 0.65, and 0.73, respectively. Other parameters are fixed as Ar=2.7, ρ_l=1200 kg/m^3, ρ_g=1.0 kg/m^3, μ_l=68 cP, μ_g=0.01 cP, and $r_o=1.35\times10^{-3}$ m.

initial bubble growth stage, which is dominated by surface tension. After the transition points, the bubble top rises much faster in the lower-viscosity liquid than in the higher-viscosity liquid. At the beginning stage of the bubble growth, since the velocity is small and so is the velocity gradient, the viscous force is small compared to other forces like buoyancy and surface tension forces. When the necking occurs, the velocity near the neck region becomes large, and so does the velocity gradient. Hence, the balance of viscous force and surface tension is important in controlling the necking process during bubble pinch-off. Zhang and Stone [23] also pointed out that the viscous force only has a significant effect at a late stage near pinching. Hence, the viscous force is significant at the necking stage for finite viscosity, and slows down the necking and pinch-off. It should also be pointed out that for the low-viscosity cases, such as $\mu_l<17$ cP, the viscosity effect on the top rising distance is minimal in this study, while for the high-viscosity case, the effect is significant.

The effect of liquid viscosity on the size of the bubble pinched off is one of the most interesting research topics over decades and has been investigated by a number of researchers. An extensive review on this topic was given by Kulkarni and Joshi [29]. The experimental results by various researchers have indicated different views [29], and these views are that (1) the bubble size increases with the liquid viscosity; (2) the liquid viscosity does not affect the bubble size; (3) the effect of the liquid viscosity on bubble size is weak; and (4) in the condition of a low flow rate, the bubble size does not depend on the liquid viscosity for a liquid with low viscosity, while a larger viscosity results in a greater bubble for the liquid with high viscosity. Figure 9 shows the numerical predictions for the effect of the liquid viscosity on the created bubble volume, where the bottom horizontal axis shows for the viscosity μ_l, and the top horizontal axis denotes the Archimedes number Ar. It is clear that the change of the bubble volume is minimal for low liquid viscosity, while the bubble volume increases with the liquid viscosity when it is high enough. As the flow rate is very low in our simulations, our observations agree with the above view (4) of Siemes and Kaufmann [30]. Because the viscosity tends to slow down the bubble breakup for high viscosity as mentioned in the last section, there will be more gas accumulated in the bubble for the higher-viscosity cases, and thus a larger bubble is created. It should be noted from Fig. 9 that the volume changes very sharply at viscosity greater than 68 cP, and this sharp transition again indicates that the viscous forces are becoming dominant for high-viscosity cases.

C. Surface tension effects

It is obvious that the surface tension is one of the important factors affecting the bubble pinch-off. In order to study the surface tension effect on bubble pinch-off, the surface tension coefficient is varied from 5 to 120 mN/m while the other fluid properties are kept constant. It should be noted that for each simulation the surface tension coefficient is assumed to be uniform on the bubble surface. As a result, all the nondimensional parameters will remain constant except the Bond number. For all the simulations, Ar=2.74, and the viscosity and density ratios are $\eta=1.5\times10^{-4}$ and $\lambda=8.3\times10^{-4}$, respectively.

Figure 10 depicts the variation of the bubble neck radius versus time before pinch-off under different surface tension coefficients, i.e., σ=15, 30, 60, and 120 mN/m. The corresponding Bond numbers Bo are 1.43, 0.71, 0.36, and 0.18, respectively. The bubble necking radius decreases with time as a power law for all four cases as the fitted lines are straight in a log-log plot (as shown in Fig. 10). It can be seen

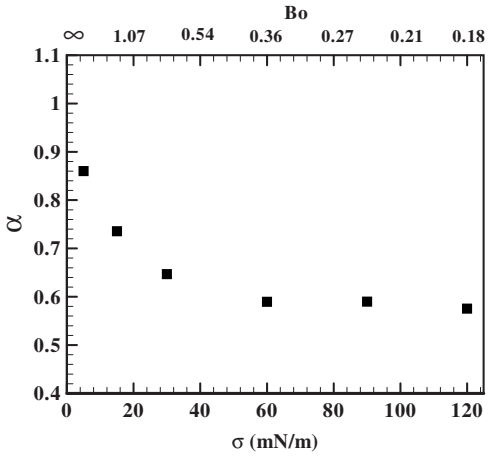

FIG. 11. Effect of surface tension coefficient on the power law exponent (α). The top horizontal axis indicates the corresponding Bond number (Bo). Other parameters are fixed as Ar=2.7, ρ_l=1200 kg/m^3, ρ_g=1 kg/m^3, μ_l=68 cP, μ_g=0.01 cP, and $r_o=1.35\times10^{-3}$ m.

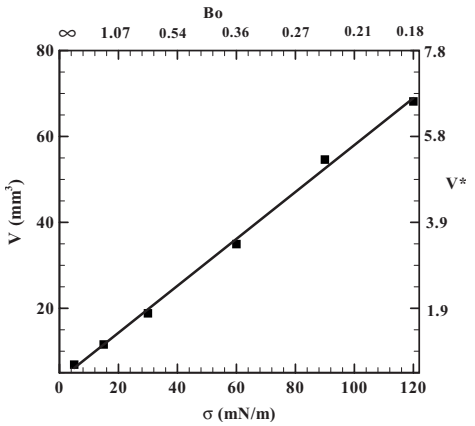

FIG. 13. Variation of bubble volume versus the surface tension coefficient (σ) and Bo. The nondimensional volume (V^*) is also shown, and it is nondimensionalized by the volume of a sphere with the nozzle exit radius. Other parameters are fixed as Ar=2.7, ρ_l=1200 kg/m^3, ρ_g=1 kg/m^3, μ_l=68 cP, μ_g=0.01 cP, and $r_o=1.35\times10^{-3}$ m.

that the surface tension tends to shorten the bubble necking process. The slopes for the four fitted lines from top to bottom at 0.58, 0.59, 0.65, and 0.73, respectively. Figure 11 shows the effect of the surface tension coefficient on the power law exponent α, where the corresponding Bond number is plotted on the top x axis. It should be noted that Bo is infinity at the left edge of the graph when $\sigma\rightarrow0$. It can be seen that there is a sharp decrease of the power law exponent α with increasing surface tension when $\sigma<30$ mN/m, and an almost constant power law exponent ($\alpha\approx0.56$–0.6) when $\sigma>60$ mN/m. The transition region occurs when $30<\sigma<60$ mN/m, which corresponds to Bo=0.72–0.36, around $O(1).$

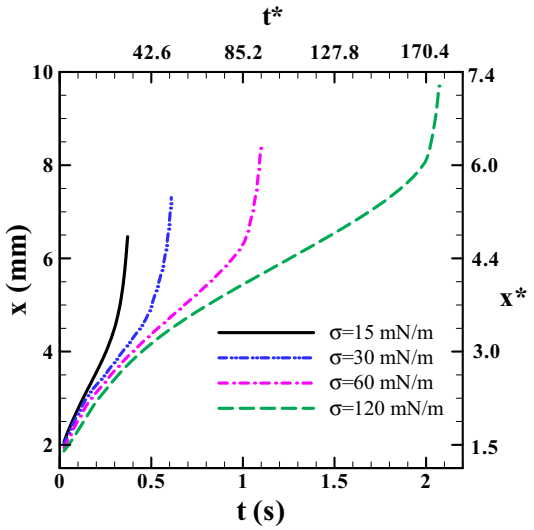

FIG. 12. (Color online) The effect of surface tension on the bubble top rising distance while pinch-off. The nondimensional time (t^*) and top rising distance (x^*) are also shown. The corresponding Bond numbers are 1.43, 0.71, 0.36, and 0.18. Other parameters are fixed as Ar=2.7, ρ_l=1200 kg/m^3, ρ_g=1.0 kg/m^3, μ_l=68 cP, μ_g=0.01 cP, and $r_o=1.35\times10^{-3}$ m.

Figure 12 shows the bubble top rising distance for the four different cases. Unlike the liquid viscosity, the surface tension affects the top rising distance from the beginning stage as the bubble grows. There also is a transition point for each of the four curves, and this transition indicates the beginning of the necking. The surface tension retards the transition point in a very noticeable manner, as seen from this figure.

The surface tension effect on the generated bubble volume is also a very interesting subject, as reviewed by Kulkarni and Joshi [29]. A number of correlations for bubble size with respect to the surface tension have been proposed. As discussed in the last paragraph, the surface tension significantly affects the bubble pinch-off process, and thus the bubble volume. Figure 13 shows the variation of bubble volume versus the surface tension coefficient, and it can be seen that the relationship between the volume of the bubble and the surface tension coefficient is almost linear, which agrees with Middleman's theoretical solution [31]. By assuming very slow motion and a static equilibrium of the droplet, Middleman found that the force balance of the droplet dripping off from a tube by gravity is $\rho_l g V=\sigma\ 2\pi r_o\cos\theta$, where θ is the contact angle. By further assuming that the drop falls off at $\theta=0$, he found that the volume of the created drop is linearly proportional to the surface tension coefficient, i.e., $V=2\sigma\pi r_o/\rho_l g$. Our prediction for the relationship of the bubble size with the surface tension also agrees with the correlation given by Tsuge and co-workers for bubble formation from a submerged orifice [32,33].

D. Density effects

We have shown in the previous sections that both the viscosity and the surface tension significantly influent the bubble pinch-off process. Here, we shall investigate the effects of the density of the bubble phase on the bubble pinch-off process. As the Bond number is a function of the density difference, the density of the bubble phase is varied in such a

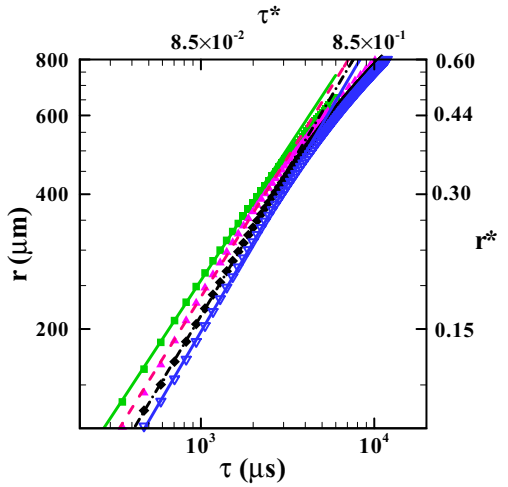

FIG. 14. (Color online) Effect of bubble density on the bubble neck shrinkage with time during pinch-off. The nondimensional time (τ^*) and radius (r^*) are also shown. The bubble density is varied at ρ_g=1.0 (■), 10.0 (▲), 50.0 (♦), and 100 (▼) kg/m^3, and the corresponding density ratios are 8.3×10^{-4}, 8.3×10^{-3}, 4.2×10^{-2}, and 8.3×10^{-2}. Other parameters are fixed as Ar=2.7, Bo=0.36, ρ_l=1200 kg/m^3, μ_l=68 cP, μ_g=0.01 cP, and r_o=1.35 $\times10^{-3}$ m.

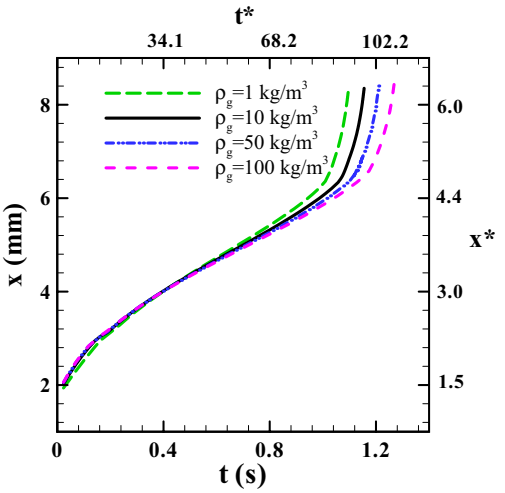

FIG. 15. (Color online) Effect of bubble density on the top rising distance of the bubble pinch-off. The nondimensional time (t^*) and top rising distance (x^*) are also shown. The corresponding density ratios are 8.3×10^{-4}, 8.3×10^{-3}, 4.2×10^{-2}, and 8.3×10^{-2}. Other parameters are fixed as Ar=2.7, Bo=0.36, ρ_l=1200 kg/m^3, μ_l=68 cP, μ_g=0.01 cP, and r_o=1.35$\times10^{-3}$ m.

way that the change in the Bond number is not noticeable. The bubble phase densities are chosen to be 1.0, 10.0, 50.0, and 100.0 kg/m^3. The liquid phase density is kept constant as 1200 kg/m^3. Hence, the density ratios are 8.3×10^{-4}, 8.3×10^{-3}, 4.2×10^{-2}, and 8.3×10^{-2}, respectively. A modified Bond number is introduced as $\mathrm{Bo}'=(\rho_l-\rho_g)gr_o^2/\sigma$, and the effect on the modified Bond number is small as the density ratios are less than 10%. For all the simulations, Ar =2.74, and Bo is around 0.36.

Figure 14 shows the neck radius versus time for the four different gas densities. The four results are very close, and this suggests that the gas density has a minimal effect on the necking process. The bubble top rising distance versus time is displayed in Fig. 15. Again, the density does not affect the top rising distance very much. These two figures imply that the gas phase density will not affect the volume of the created bubble. It is no surprise that the bubble volumes for the four cases are 15.4, 14.7, 14.9, and 15.5 mm^3. Thoroddsen *et al.* [8] studied the bubble density effect on the pinch-off process by using two different gases, namely, He and SF_6, and also found that the effect of the density on the breakup is negligible.

IV. CONCLUSION

A numerical investigation of a low-viscosity gas bubble pinch-off in a more viscous liquid is presented. The numerics used a finite-volume method coupled with a front tracking scheme to capture the interface. The numerical schemes are validated by comparison to previous experimental results. The necking radius decreases with time in a power law mode, which agrees with previous experimental investigations. The effects of the liquid phase viscosity, the surface tension coefficient, and the bubble phase density on the bubble pinch-off were studied. Our results showed that both the viscosity and surface tension coefficient have significant effects on the bubble pinch-off. Higher viscosity and surface tension coefficients tends to retard the necking process, and thus create a larger bubble, while the density of the bubble phase plays a minimal role on the bubble breakup. The power-law exponent is affected not only by the liquid viscosity, but also by the surface tension coefficient. In addition, our simulation results show that the significant transition of the power law exponent occurs at Ar=0.37–2.7 of $O(1)$ when the viscosity is varied, and at Bo=0.36–0.72 of $O(1)$ when the surface tension coefficient is varied.

ACKNOWLEDGMENTS

The authors would like to express their grateful thanks to Professor S. T. Thoroddsen from the National University of Singapore for providing us with the valuable experimental data on bubble pinch-off so that the detailed validation of our numerical simulation was possible. We are also grateful to the referees for their valuable suggestions and constructive comments.

[1] J. Eggers, Rev. Mod. Phys. **69**, 865 (1997).
[2] I. Cohen and S. R. Nagel, Phys. Fluids **13**, 3533 (2001).
[3] A. U. Chen, P. K. Notz, and O. A. Basaran, Phys. Rev. Lett. **88**, 174501 (2002).
[4] J. C. Burton, J. E. Rutledge, and P. Taborek, Phys. Rev. Lett. **92**, 244505 (2004).
[5] P. Doshi, I. Cohen, W. W. Zhang, M. Siegel, P. Howell, O. A. Basaran, and S. R. Nagel, Science **302**, 1185 (2003).
[6] N. C. Keim, P. Moller, W. W. Zhang, and S. R. Nagel, Phys. Rev. Lett. **97**, 144503 (2006).
[7] J. C. Burton, R. Waldrep, and P. Taborek, Phys. Rev. Lett. **94**, 184502 (2005).
[8] S. T. Thoroddsen, T. G. Etoh, and K. Takehara, Phys. Fluids **19**, 042101 (2007).
[9] M. S. Longuet-Higgins, B. R. Kerman, and K. Lunde, J. Fluid Mech. **230**, 365 (1991).
[10] H. N. Oguz and A. Prosperetti, J. Fluid Mech. **257**, 111 (1993).
[11] H. Wong, D. Rumschitzki, and C. Maldarelli, J. Fluid Mech. **356**, 93 (1998).
[12] S. Sierou and J. R. Lister, J. Fluid Mech. **497**, 381 (2003).
[13] J. Eggers, M. A. Fontelos, D. Leppinen, and J. H. Snoeijer, Phys. Rev. Lett. **98**, 094502 (2007).
[14] J. M. Gordillo, A. Sevilla, J. Rodriguez-Rodriguez, and C. Martinez-Bazan, Phys. Rev. Lett. **95**, 194501 (2005).
[15] J. M. Gordillo and M. Perez-Saborid, J. Fluid Mech. **562**, 303 (2006).
[16] R. Bergmann, D. van der Meer, M. Stijnman, M. Sandtke, A. Prosperetti, and D. Lohse, Phys. Rev. Lett. **96**, 154505 (2006).
[17] J. Rodriguez-Rodriguez, J. M. Gordillo, and C. Martinez-Bazan, J. Fluid Mech. **548**, 69 (2006).
[18] R. Suryo, P. Doshi, and O. A. Basaran, Phys. Fluids **16**, 4177 (2004).
[19] D. Gerlach, N. Alleborn, V. Buwa, and F. Durst, Chem. Eng. Sci. **62**, 2109 (2007).
[20] G. Tryggvason, B. Bunner, A. Esmaeeli, D. Juric, N. Al-Rawahi, W. Tauber, J. Han, S. Nas, and Y. J. Jan, J. Comput. Phys. **169**, 708 (2001).
[21] J. Hua and J. Lou, J. Comput. Phys. **222**, 769 (2007).
[22] J. Hua, B. Zhang, and J. Lou, AIChE J. **53**, 2534 (2007).
[23] D. F. Zhang and H. A. Stone, Phys. Fluids **9**, 2234 (1997).
[24] S. I. Abarzhi, K. Nishihara, and R. Rosner, Phys. Rev. E **73**, 036310 (2006).
[25] C. S. Peskin, J. Comput. Phys. **25**, 220 (1977).
[26] C. S. Peskin and B. F. Printz, J. Comput. Phys. **105**, 33 (1993).
[27] S. V. Patankar, *Numerical Heat Transfer and Fluid Flow* (Hemisphere, New York, 1980).
[28] T. Bonometti and J. Magnaudet, Phys. Fluids **18**, 052102 (2006).
[29] A. A. Kulkarni and J. B. Joshi, Ind. Eng. Chem. Res. **44**, 5873 (2005).
[30] W. Siemes and J. F. Kaufmann, Chem. Eng. Sci. **5**, 127 (1956).
[31] S. Middleman, *Modeling Axisymmetric Flows: Dynamics of Films, Jets, and Drops* (Academic Press, New York, 1995).
[32] H. Tsuge, Y. Nakajima, and K. Terasaka, Chem. Eng. Sci. **47**, 3273 (1992).
[33] H. Tsuge, K. Terasaka, W. Koshida, and H. Matsue, Chem. Eng. Sci. **52**, 3415 (1997).